Pulsatile therapy for perovskite solar cells

Mansoo Choi (mchoi@snu.ac.kr)
Seoul National University https://orcid.org/0000-0003-3198-6899
Kiwan Jeong
Global Frontier Center for Multiscale Energy Systems
Junseop Byeon
Seoul National University
Jihun Jang
Global Frontier Center for Multiscale Energy Systems
Namyoung Ahn
Global Frontier Center for Multiscale Energy Systems

Physical Sciences - Article

Keywords: renewable energy, solar energy, pulsatile therapy, perovskite materials

Posted Date: February 16th, 2021

DOI: https://doi.org/10.21203/rs.3.rs-209220/v1

Abstract

Although photovoltaics employing hybrid perovskite halides have continuously been breaking world-records of power conversion efficiency (PCE) and expectations for their industrialization are rapidly rising, long-term stability issue that has greatly hampered the commercialization of perovskite solar cells has not been resolved yet. Ion instability and trapped charges were suggested as a fundamental reason for perovskite device degradation. Here, we report a pulsatile therapy relieving the accumulation of both trapped charges and ions in the perovskite solar cell device during the middle of maximum power point tracking (MPPT) for reviving the device and prolonging its device lifetime. In the technique, reverse biases are repeatedly applied for a very short time to eliminate the charges accumulated and re-distribute the ions migrated during power harvesting without any pause of operation. Intriguingly, the therapy is not only delaying irreversible degradation, but also, restoring the degraded power right after a short reverse bias. In-situ photoluminescence (PL) and photocurrent (PC) measurements for the working device were done while applying the pulsatile therapy for studying the underlying physics. Time evolving PL intensity and PC not only revealed the steady increase of PL intensity during the therapy indicating the reduction of non-radiative recombination, but also strikingly showed the restoration of degraded PL intensity and PC right after a short reverse bias suggesting the device healing. In the long-term test, we observed outstanding improvement of device stability and total harvesting power. A model considering trap-assisted recombination has also been developed to explain the efficacy of the therapy based on defect formation during MPPT operation and defect healing by the pulsatile therapy. The unique technique will open up new possibility to commercialize perovskite materials into a real market.

Introduction

Perovskites can be utilized for a wide range of applications like flexible and wearable power sources[12,13], tandem devices with Si solar cells[14], also other photonic devices such as light emitting diodes[8,14] and photodetectors[15,16]. However, real markets will require insurance for a long-term operational stability of perovskite devices and unfortunately, the insurance of lifetime has not been guaranteed yet[17] . The current level on device stability is just about few thousands of hours under one sun light illumination and the understanding on fundamental mechanism of perovskite device degradation is still limited.

As part of an effort to solve this stability issue of perovskite solar cells, many studies were performed. Degradation studies picked up ion instabilities and trapped charges as the main reason of perovskite instabilities[9-11]. Ions are easily migrated through defect sites by electric field and light illumination, leading to material transformation[18]. Although several reports showed a positive role of ion migration like defect healing [19], most of relevant studies demonstrated instabilities induced by halide migration and segregation[20-23]. Interestingly, it was confirmed that degradation induced by ion instabilities occurred somewhat reversibly. Decreased performance was recovered back after storing the degraded device in the dark chamber. But, the recovery took several hours (usually overnight) for spontaneous ion redistribution. Carrier charges trapped in perovskite films were found to induce irreversible degradation in the presence

of H_2O and/or O_2, producing stable yellow lead(II) iodide and lead hydroxide species[11,17]. Detailed chemical routes of trapped-charge driven irreversible degradation were identified via *ab initio* molecular dynamics simulation[24,25]. Oxygen driven degradation studies also suggested an important role of localized charges in the formation process of superoxides[25, 26]. It was recently confirmed that such charges play a critical role in irreversible device-level degradation[17, 27]. Ion instability was also found to be deeply involved with localized charge trapping[28]. All of these studies relevant to perovskite degradation indicate that the instability of perovskites would originate fundamentally from the accumulated charges and ions in perovskites, as well as their interplay[29,30]. Thus, the long-term stable perovskite solar cells will require the mitigation of their negative effects on degradation.

Herein, we developed a novel method (called pulsatile therapy) to revive the degraded device and lengthen its device lifetime by effectively mitigating accumulated charges and ions in the middle of maximum power point tracking (MPPT). In the therapy, a pulsatile reverse pulse (RP) bias is repeatedly applied for a very short time to eliminate accumulated charges as well as drift migrated ions reversely, leading to the stabilization of the working device. To systemize our pulsatile therapy (PT), we built a new pulsed-MPPT system that can provide desired rectangular pulse waves of bias voltage, in which the amplitudes for both MPPT and RP were programmatically calculated from feedback information of actual *I-V* characteristics of the target cell. The system demonstrated that the PT significantly improved total power harvesting and device lifetime in comparison to the normal MPPT case for different types of perovskite solar cells, though not fully optimized yet. Strikingly, it was clearly demonstrated that the therapeutic effects were not only to make device degradation slower, but to restore degraded power again after a RP.

To further elucidate the mechanism underlying our PT, we studied dynamics of photoluminescence (PL) intensity during the therapy together with photocurrent(PC) tracking from the working device. We confirmed charge extraction and ion redistribution from bi-exponential fitting of PL intensity and PC signals during the reverse bias step, which also accompanied steady rise of PL intensity indicating suppression of non-radiative recombination. In the following MPPT step, both PL intensity and PC restored from their degraded values again, which is a clear evidence of device healing. Our PT led to improvement of total harvested energy by up to 11.3% for 500 h-long operation compared to continuous MPPT operation. It was reproducibly confirmed that all devices of different structures operating with PT showed better stability and energy generation than MPPT-devices. This technique is the first method to heal the device without any pause of operation, as well as effectively improve total harvested energy regardless of inherent device quality and stability.

Dependency of electrical operation conditions on device degradation

First, we investigated device stability under light soaking depending on different electrical conditions (short-circuit (SC), maximum power point tracking (MPPT), and open-circuit (OC), respectively). (See **Fig. 1a**) Although configurations and photovoltaic parameters of each device were different, the fastest degradation among three conditions was observed always when the device was kept open-circuited.

Detailed information about those devices is described in **Extended Data Fig.1**. Both MPPT and SC conditions showed slower degradation than the OC condition, but the most stable operation was observed in the case of the SC condition. Such bias dependency of the degradation speed was also reported in previous degradation studies[31,32]. We additionally compared device stability depending on four different applied biases (**Fig. 1b**). The result revealed that higher applied voltage led to faster device degradation. We observed extremely stable operation for total 100 hours under both 0.5V and 0.65V of applied biases (less than the initial MPP bias), while devices operating under higher voltage experienced significant drop of normalized power. It is notable that all stable cases (SC, 0.5V and 0.65V) have current densities equivalent to short-circuit current (J_{sc}), which indicates that if a sufficient current flows, a device can work very stably. (see **Extended Data Fig.2**) On the contrary, when current extraction was impeded by potential barrier in all unstable cases (OC, 0.75V, and 0.8V), fast degradation of photocurrent occurred (**Extended Data Fig.2a**). As shown in **Extended Data Figs.2b-c**, the best condition in terms of total power generation is 0.65V of applied voltage which is lower than the initial MPP bias (~0.75V) of the device (in this condition, the current density is about 97% of J_{sc}). Together with these bias-dependent stability data, the fact that the charge accumulation in the device should be the largest for the OC case showing the fastest degradation and the smallest for the SC case showing the highest stability would be consistent with previous reports[11,29] that suggested the trapped charges and bias dependent ion migration as fundamental reasons for the degradation of perovskite solar cells (see the overall illustration in **Fig. 1c**.). The overview of previously reported mechanisms for perovskite degradation is summarized in **Supplementary Information Section A.** To deal with these fundamental reasons, a pulsatile therapy that eliminates the charges accumulated and re-distributes the ions migrated during the power harvesting process via repeated reverse biases is developed in the present study for the first time.

A pulsatile therapy and its efficacies

An interesting observation is that operational stability also depends on time interval of *I-V* sweeps as presented in **Extended Data Fig.3**. The shorter time interval (5 min) led to better stability than the longer interval (30 min). Those imply not only that the duration of MPPT operation may affect the operation stability, but that *I-V* sweeps may also slow down device degradation by releasing accumulated charges and migrated ions during *I-V* sweep process. This confirms again that electrical operation conditions for these sensitive perovskites, play a critical role in operational stability. Focusing on an electrical technique to ease two fundamental reasons, we developed a pulsed-MPPT system to lengthen device lifespan and harvest more power, which is practically applicable without stopping operation. To extract the charges accumulated and re-distribute ions migrated during a period of MPPT operation, a short reverse pulse (RP) bias is applied periodically by our programmed algorithm in our pulsed-MPPT system. (See **Fig. 2a**) Our system was specially developed to provide a fully automatic pulsed-MPPT by sending and receiving continuous feedbacks between tested devices and the system. (See **Methods**) Based on a simple circuit model including a capacitance taking into consideration the accumulation of charges (**Supplementary Information Section B**), the value of applied RP bias is chosen to eliminate potential difference across a

perovskite intrinsic layer and updated periodically, thereby, we can obtain optimal pulse amplitude for our pulsatile tracking system.

Fig. 2b shows an applied pulse wave of bias voltage and corresponding photocurrent (PC) values over time of a device operated by this system. *I-V* curves are obtained periodically to estimate photovoltaic performance of the tested device. As mentioned earlier, this system uses recently-updated *I-V* characteristics to calculate MP and pulse bias. During power harvesting, applied bias over time will be a simple pulse wave (rectangular wave) that has an amplitude of maximum power voltage(V_{MP}) in a forward bias. In the RP process with an amplitude of V_{RP}, electrical power will be consumed to apply RP, but energy loss will be far lower than energy harvesting as weak reverse biases are applied for a much shorter time than energy harvesting process. Energy losses occurred during RP are strictly included for precise comparison. We will call this operational method as pulsatile therapy (PT). To fairly evaluate the efficacy of PT, we prepared four cells in one ITO-patterned glass that are electrically independent by additional ITO etching. (see **Methods**) As each cell was fabricated through the same process on one substrate, all these cells were very similar in terms of performance and degradation. It was confirmed from the test results obtained for four pixels as shown in **Extended Data Fig.4**.

We tested the efficacy of PT for Cs-doped $FA_{0.92}MA_{0.08}PbI_{3-x}Br_x$ perovskite solar cells with 20% of PCE (ITO/SnO_2/perovskite/Spiro-MeOTAD/Au). For the first PT test, its time width for MPPT(T_{MP}) and RP(T_{RP}) was fixed at 30 minutes and 30 seconds, respectively. Standard MPPT was simultaneously performed for the other identical cell in the device. **Fig. 3a** shows time evolution of normalized power for PT- and MPPT-tested cells. While normalized power of the cell with PT maintained 93% of the initial power in 40 hours, that of the MPPT-cell decrease by 89.5% of the initial power (will show later for a long term operation). To verify RP effect on device performance, we observed kinetics of normalized power before and after a RP during 2-3 h and 16-17 h. **Fig. 3b** shows that normalized power linearly decreased for both MPPT and PT cases, in which the decay speed of the PT (0.97 $\%h^{-1}$) was slower than that of the MPPT case (1.31 $\%h^{-1}$). Namely, the PT slows degradation down, which is the first efficacy of the PT. After some progression of degradation (16 h), we could observe another signal to show its efficacy. As can be seen in **Fig. 3c**, degraded power during MP was dramatically restored shortly after a RP, whereas the recovery was not observed in MPPT operation**.** The PT-induced recovery looks similar to self-healing in dark conditions for overnight[33-35]. An intriguing point is that our PT can restore degraded performance in just 30 seconds without pause of operation. The recovery is shown to become pronounced with aging, which would be attributed to the recovery from ion defects increased with time by the reverse biases. Even though there is no pronounced PC recovery observed at early times, a clear improvement of the stability is still shown in **Fig. 3b** in comparison to MPPT case, which suggests that the reverse bias pulses (RPs) effectively extract the charges accumulated during MPPT operation that could mitigate trapped-charge driven irreversible degradation[11,24,25]. Interestingly, these short-term experimental results shown in **Fig. 3b-c** tell that our PT having periodic reverse biases effectively works for the practically fresh devices by not only slowing down the irreversible degradation caused fundamentally by trapped charges, but also healing the

degraded device caused by ion defects formed with time somewhat in a reversible way. (We will discuss detailed mechanism and long-term effects of our PT later)

As clinical trials on the PT, pure $MAPbI_3$ solar cell employing vapor-deposited C_{60} ETL was also tested in the same way. (see **Extended Data Fig.5a**) Device stability was improved by PT, and the kinetics of normalized power over time were similarly observed in terms of photocurrent recovery after RPs. (**Extended Data Fig.5b-d**) That indicates the PT can work for different types of perovskite solar cells.

Mechanism of defect healing by pulsatile therapy

To reveal the mechanism underlying PT efficacies, we customized PL setup to detect time evolution of PL emission from the device controlled by PT as illustrated in **Fig. 4a**. The desired voltage bias can be applied by a LabVIEW-controlled electro source meter (Keithley 2400) and PC flowing through the measured device will be recorded at the same time. Continuous irradiation of 150W Xe lamp was used to excite our sample for PL detection. (~ 75 mW/cm^2 on a target sample). We also measured steady-state PL of our device under different bias voltage (**Extended Data Fig.6a**) The PL signals increased as we increased the bias voltage, which indicates that radiative recombination happened more at a higher bias due to augmented remaining photo-generated charges. PL intensities at the peak position of 778 nm were plotted as a function of bias voltage under both forward and reverse voltage sweep (**Extended Data Fig. 6b)**. The *PL-V* curves, which look similar to normal *I-V* curves, show an effect of bias voltage on carrier concentration in a light-illuminated device suggesting that our PL setup stably works for a working device under both light illumination and electrical bias.

Using the new setup, we investigated the kinetics of PL and PC during MPPT operation for over 1h (see **Fig. 4b**). We observed the extremely steep decay of PL and PC signals appearing at the beginning of the measurement, which was due to transient change of applied bias and light excitation. After the fast transient decay, still continuous decreases of both PL intensity and PC were observed until the end of the measurement. It literally indicates a degradation of the perovskite device during MPPT operation. Accompanied decrease of PL intensity could be explained by the augmentation of deep-level defects where non-radiative recombination occurs [30,36]. In the early stage before 1000 seconds, PC decrease took place more badly than PL, which could be attributed to ion accumulation to form a barrier of charge extraction[37]. We also detected time-evolving PL intensity and PC for 30 seconds during a RP applied after 30 minutes of MPPT operation (see **Fig. 4c**). Both PC and PL intensity dynamics induced by a short RP are well fitted by bi-exponential functions with similar time-constants (see **Extended Data Table.1**), of which the fast one results from capacitive current due to discharging of accumulated charge and the slow one indicating field-induced ion movement[38]. The increase of PL intensity during the RP shown in **Fig. 4c** points out that non-radiative recombination is reduced during 30 sec of RP (see the black and blue arrows in **Fig. 4d**), which is indicative of defect healing (see more details in **Supplementary Information Section C)**. Clear evidence of defect healing by RPs is shown in overall kinetics of PL intensity and PC during one cycle of PT (MP→RP→MP). (see **Fig. 4d**) It was confirmed that both PL intensity and PC were saturated at higher values than the values at the last minute of the previous MP process, which is

consistent with recovery of normalized power after RPs shown in **Fig. 3c**. The kinetics were confirmed reproducibly, even in the case of shorter or longer RPs (**Extended Data Fig.7**) These results tell that the RP effectively extracts carrier charges and releases ion accumulation without any pause of operation, finally leading to the defect annihilation and the reduction of non-radiative recombination. Therefore, the PT stabilized the damaged device again after every RPs, thereby device degradation was delayed and performance recovery occurred. Note that photocurrent recovery after RPs could be almost invisible during the measurements depending on device status (**Fig. 3b-c**), as the magnitude of photocurrent recovery depends on the level of ion defects. Even in the case, defect healing may always take place during the PT, which was evidenced from the discernible recovery of PL intensity. Previously reported defect dynamics[30,39-42] could explain our observations of PT. When a perovskite device operates at MPPT under light illumination, charge carriers, ions, and defects in a perovskite film will start to move by diffusion-drift model[43]. Carriers will be transferred to corresponding transporting layer by diffusion, resulting accumulation of trapped carriers at the interface (trapped electron near PSK/ETL interface, trapped hole near PSK/ HTL interface). Ions will migrate to compensate internal electric field(drift motion), resulting accumulation near interface(Pb_i^{2+}, I_i^+ near PSK/ETL interface, I_i^- near PSK/HTL interface)[43,44]. As a result, both carriers and ions could be localized at both interfaces, leading to device degradation. The localization can be even severe due to Coulombic interaction between carriers/ions. In this condition, the formation energies of I_i^0 and Pb_i^0 become lower than those of $I_i^{-1}$and Pb_i^{2+}, which means that charge-state transition can be energetically favorable as the following reactions.[30,39,40]

$$I_i^- + h^+ \leftrightarrow I_i^0 \quad I_i^+ + e^- \leftrightarrow I_i^0 \ldots (1)$$

$$Pb_i^{2+} + 2e^- \leftrightarrow Pb_i^0 \ldots (2)$$

Such reactions happen slowly, but steadily during MP operation. The neutral interstitial defects (I_i^0, Pb_i^0) occupy deep-level states within bandgap, which supply sources of non-radiative recombination[45]. As a result, both PL intensity and PC decrease as shown in **Fig. 4b**. The degradation continues as long as the MP operation is maintained. However, the PT has special steps to apply reverse pulses periodically. If a RP is instantaneously applied during our PT, carriers and ions will reversely move from the previous MP step. As a result, the charge-state transition will occur oppositely because the neutral interstitial defects are no longer energetically favorable when electrons or holes vanish out by the RP. Therefore, deep-level defects could return to shallow defects like I_i^{-1} and Pb_i^{2+} again, which well explains our observation of defect healing in our PT. We discuss in detail on overall process and all possible scenario underlying PT in **Supplementary Information Section C**.

Long-term effect of pulsatile therapy

To evaluate technical value of our PT, we estimate total gain that corresponds to how much total energy harvested by PT relatively improve over MPPT. (**Supplementary Information Section D**). Total gain is time-dependent because efficiency continuously changes and power consumption during RPs should be

considered together. Total gain at the early stage of PT will be always negative due to the power consumption needed for RPs. However, if the PT works, total harvested energy of PT will catch up that of MPPT as time goes on. If total gain finally exceeds 0%, PT is technically meaningful. That is, we can exactly evaluate the therapeutic effect of our pulsatile therapy in terms of total energy harvesting using total gain. **Extended Data Fig.8** shows total gain versus time of the short term (40 h) test of PT shown in **Fig.3**. After 40 hours of PT operation, total gain was -0.2%, which means the PT was not still effective in the short-term operation. (power consumption for RPs exceeds power gain acquired by the stability improvement for this short period)

We additionally conducted long-term test under continuous light illumination for 500 h. A new PT condition (MP:RP =10 min:2 sec) was added in this test to reduce power consumption for RPs. **Fig. 5a** presents three profiles of normalized power as a function of time for MPPT, the previous PT condition (PT1), and the new PT condition (PT2). Both PT conditions show better stability compared to MPPT and the effect became pronounced. After 500 h of operation, PT1 and PT2 maintained 79.2% and 76.9% of their initial power, respectively, while MPPT maintained 72% of its initial power. Differences in normalized power for three conditions became pronounced after about 65 h of continuous operation, especially only PT1 kept relatively stable operation. This points out that 2 second reverse biases for PT2 would be sufficient to cause charge extraction, but not ion redistribution, whereas 30 sec of RP for PT1 is more effective for both charge extraction and ion redistribution, leading to the best stability. We estimated total gain for two PT conditions as shown in **Fig. 5b**. Both PT1 and PT2 achieve 5.44% and 3.58% of total gain at 500 h compared to MPPT case, respectively. The trend of total gain is still growing at 500 h and total gain can be further improved for longer operation. It is noteworthy that total gain of PT2 reached the threshold at 5.8 h, which was much faster than that of PT1 (110.9 h). This means that PT2 with shorter RPs is more effective than PT1 in the short-term, although PT2 was overtaken by PT1 at 158 h. Since ion migration may become active as aging progresses, ion redistribution in degraded devices requires longer RPs to sufficiently mitigate accumulation of charges and ions. So, the PT1 with longer RPs showed far better stability than PT2 in the case of long-term operation.

Taking advantage of PT2 that is more effective for short-term, we tested a mixed PT, in which PT2 was applied first, and converted to PT1 after 65 h. **Fig. 5c** shows normalized power profile of MPPT, PT1, and mixed PT (PT3) for 500 h. Both PT1 and PT3 led to better stability than MPPT, as consistently confirmed in this present work. Interestingly, two profiles for PT1 and PT3 look different before 65 h, however, those have very similar trend after it was changed from PT2 to PT1. At 500 h, both PT1 and PT3 maintained 72.3% of their initial power, while only 62% of the initial power was retained in the MPPT case. Please note that the gear-like shape in the profile of PT3 at 250h to 500h happened from sudden changes of maximum power point after a *I-V* sweep, not from device instability. We also estimated total gain for PT1 and PT3 in this test set as shown in **Fig. 5d**. Although PT3 started with better total gain due to low power consumption for RPs, total gain of PT1 catch up with that of PT3 at 300 h. PT1 achieved total gain of 11.3% at 500 h, which is slightly higher than 10.8% of total gain in the case of PT3. The estimation of total gains for different designs of PT reveals that our pulsatile therapy works very reproducibly for device stability. Note that PT can be designed in a flexible way, therefore, it would be possible that an extremely

stable operation could be designed depending on device conditions and operation time, in which every RPs can be differently applied by real-time feedback and analysis.

We additionally investigated time evolution of *I-V* curves for MPPT, PT1, and PT3, respectively (**Fig. 5e-g** and **Extended Data Fig.9).** Initial *I-V* curves of all cases look normal. But, as degradation continued, a peculiar shape of *I-V* curves (twice-deflected) started to appear only in the case of MPPT after 200 h of operation, while *I-V* curves for PT1 and PT3 continuously keep their typical diode shapes. (see **Fig. 5e-g**) In the peculiar *I-V* curves, there exist two clear deflections points at around 0.5V and 0.9V, respectively. (see green circles in Fig. 5e) It was clearly confirmed by *Conductance-Voltage* curve, where conductance is defined in differential sense (conductance = $|dI/dV|$). A sudden jump of conductance appeared at the first deflection point (0.5V) and conductance became flat between two deflection points (see green box and dashed lines in Fig. 5e). The anomalous behavior appearing at the deflection points simply results from significant loss of photo-generated carriers rather than photocurrent extraction, indicating changes in carrier dynamics and photocurrent pathways. This could be interpreted as a result of an activation of an additional diode from the viewpoint of electrical circuit. In this sense, we conducted a circuit modeling for all *I-V* curves based on double-diode modeling[46,47]. (Our in-depth modeling is included in **Supplementary Information Section E)** The modeled electrical circuit is shown to well simulate the peculiar *I-V* curves (shown in MPPT case) which are well matched with the measured curves. According to our modeling, the peculiar shape likely originates from the emergence of a trap-assisted recombination pathway as modeled by secondary non-radiative diode and resistance[46,47]. An increase of traps during MPPT operation lets trap-assisted recombination happen more and easier, leading to lowering the resistance and increasing carrier losses at secondary diode. That is, the modeling suggests that continuous MPPT operation induced the formation of defect acting as trap-site, leading to twice-deflecting *I-V* curve. On the other hand, PT can not only suppress charge trapping but also mitigate the formation of defects as a result of charge extraction and ion redistribution, which would be why we observed the normal shape of *I-V* curves even at 500 h of operation in the case of both PT1 and PT3.

In conclusion, our PT is the first technology to cure degraded perovskite solar cells by applying a short electrical pulse of RP without any pause of operation. We confirmed that the therapy can not only delay trapped charge driven irreversible degradation, but also effectively heal damaged devices in a reversible way by extracting charges and redistributing ions. Both MA- and FA- perovskites were clinically tested, showing similar efficacies that led to slowing down their degradation speed as well as recovering degraded power reversibly. Our PT shares its special efficacies with those by self-healing in dark, but appears rapidly just in a few seconds, which makes itself energy-friendly. We verified from PL measurements that the PT suppressed the formation of harmful defects and even induced defect healing by mitigating accumulation of charges and ions, finally leading to recovery of photocurrent and delay of device degradation. Through this novel operational method, we finally achieved 11.3% of total gain after 500 h of operation in terms of total harvested energy. Its efficacy was also reproducibly confirmed in 500 h long-term test even for different PT conditions. Based on our *I-V* modeling, trap-assisted recombination could be possibly suppressed by the pulsatile therapy for 500 h of continuous operation, which is well

consistent with our PL dynamics experiments. This study proposes new approach to heal perovskite solar cell devices quickly and prolong their lifetime, therefore, opens up the possibility of perovskite solar cell commercialization to be raised to the full.

Methods

Fabrication of perovskite solar cells

The Indium-doped tin oxide (ITO) glass substrate were pre-patterned by 532nm pico-second laser to insulate 4 cells in the device. The laser power was 1.9W and the scribed line width was 300um. Patterned ITO glass substrates (AMG, 9.5Ωcm^{-2}) were cleaned by sonication sequentially using acetone, isopropanol, and deionized water. For the $MAPbI_3$- based perovskite solar cells (PSCs) with C_{60} as the electron transporting layer (device 1), a C_{60} layer (35 nm) was deposited on the cleaned ITO glass substrate using the vacuum thermal evaporator at deposition rate of 0.2 Å s^{-1}. For $MAPbI_3$-PSCs with SnO_2 as the ETL(device 2), SnO_2 layer was fabricated on the ITO glass substrate by spin-coating 2.67wt% of SnO_2 colloid precursor (tin(IV) oxide, 15% in H2O colloidal dispersion, Alfa Aesar) in DI water at 4000 rpm for 30 s. The SnO_2 layer was annealed at 150 °C for 30 min. The thickness of the SnO_2 layer was around 30 nm. A precursor solutions of $MAPbI_3$ were prepared by adding 461 mg of PbI_2 (Alfa Aesar) and 159 mg of MAI (Great solar) and 78 mg of mixed adducts dimethyl sulfoxide (DMSO; Sigma-Aldrich) with 5mol% urea in 0.55 mL of *N*,*N*-dimethylformamide (DMF; Sigma-Aldrich). The solution was spin-coated on the ETL layer at 4,000 rpm for 20 s with 0.5 mL of diethyl ether dripping treatment. The film was annealed at 115 °C for 20 min. For the Triple perovskite- based PSCs with SnO_2 as ETLs (device 3), the triple perovskite was deposited by 2-step spin coating method. First, 1.25 M of PbI_2 with 5mol% of CsCl in 0.05ml of DMSO and 0.95ml of DMF was spin coated onto the ETL at 2,500 rpm for 30 s. The mixture solution of FAI:MABr:MACl (75 mg:7.5 mg: 7.5 mg in 1 ml isopropanol) was spin coated onto the CsCl/PbI2 film at 5,000 rpm for 30 s, then annealed at 150 ◦C for 20 min. In order to prepare a solution for the hole-transporting layer (HTL), 72.3 mg of spiro-MeOTAD (Merck) was dissolved in 1 mL of chlorobenzene (Sigma-Aldrich). 28.8 µL of 4-tert-butyl pyridine and 17.5 µL of lithium bis(trifluoromethanesulfonyl)imide from a stock solution (520 mg of lithium bis(trifluoromethanesulfonyl)imide in 1 mL of acetonitrile, 99.8% purity, Sigma-Aldrich) were added to the mixture solution. The HTL was formed on the perovskite film by spin-coating mixture solution at 2,500 rpm for 30 s. A gold layer with a thickness of 50 nm was deposited on the HTL by using the vacuum thermal evaporator at deposition rate of 0.3 Å s^{-1}. All spin-coating processes were carried out in a dry room (<15% relative humidity, at room temperature). Fabricated solar cells were encapsulated with glass using UV cured resin (XNR5570, NAGASE) in glove box.

Characterization

***I-V* measurement**

The current–voltage characteristics were measured by a solar simulator (Sol3A, Oriel) and a source-meter (2400, Keithley) under AM 1.5G at 100 mW cm^{-2} at room temperature inside a glove box. The light intensity was calibrated by using a Si reference cell (Rc-1000-TC-KG5-N, VLSI Standards, USA). The aperture size of PSCs is 0.0729 cm^2.

Long-term stability test with PT

The current–voltage characteristics for aging under 1-sun light illumination were measured by a solar simulator (K3000, McScience) and a source-meter (2400, Keithley). Customized JIG was designed to contact cathode/anode of each cell on each independent section of etched ITO, independently. LABView software was used to design pulsed MPPT tracking system by controlling source-meter via GPIB. The system was set to perform *I-V* sweep periodically (3hr or 5hr were selected), with scan rate of 0.06 V/s, scan range of -0.1 V~1.1 V, voltage step of 0.04 V, and both reverse/forward direction. Recent parameters for feedback (I_{sc}, V_{oc}, R_{sh}, $R_{s,}$ *FF*) were automatically updated and calculated based on averaged values of *I-V* curve for both reverse and forward direction. T_{MP} and T_P were set prior to system operation, while V_{RP} ($-I_{sc}*R_s$) and V_{MP} were calculated by updated parameters from recently measured *I-V* sweep. The system also measured and stored realtime photocurrent values, of which the sampling rate was 0.2Hz during MPPT, and 10Hz during pulse. If a *I-V* sweep and a pulse overlap, *I-V* sweep was set as the highest hierarchy.

Kinetic photoluminescence measurement

Steady-state and kinetic photoluminescence (PL) measurements were conducted using a FluoroMax-4 spectrofluorometer (Horiba). Xenon lamp(150W) was used as a light source with wavelength near 463 nm selected using spectroscope. Voltage can be applied simultaneously by wiring device to K2400. The resulting PL was measured using high-sensitivity photodetector targeting wavelength of 780 nm.

Declarations

Author contributions

M.C. and N.A. conceived the idea of the work. N.A. and M.C. developed a theory by discussing with K.J. and J.B. K.J and J.B. contributed equally to the work. K.J., J.B and N.A. conducted experiments. J.J. did substrate preparation. N.A., M.C., K.J. and J.B. designed experiments, analyzed data, participated in discussion and wrote the manuscript. M.C. led the work.

Competing interests

The authors declare no competing interests

Acknowledgements

This work was supported by the Global Frontier R&D Program of the Center for Multiscale Energy Systems funded by the National Research Foundation under the Ministry of Education, Science and Technology, Korea (2012M3A6A7054855). We sincerely thank G. Min ,Y. Jeong, and Professor J. Ha for valuable discussion and support to design our PT systems.

Data availability The datasets generated and/or analysed during this study are available from the corresponding authors on reasonable request.

Code availability The analysis codes that support the findings of the study are available from the corresponding authors on reasonable request.

References

1. A. Kojima, K. Teshima, Y. Shirai, T. Miyasaka, Organometal halide perovskites as visible-light sensitizers for photovoltaic cells. *J. Am. Chem. Soc.* **131**, 6050-6051 (2009).
2. M. M. Lee, J. Teuscher, T. Miyasaka, T. N. Murakami, H. J. Snaith, Efficient Hybrid Solar Cells Based on Meso-Superstructured Organometal Halide Perovskites. *Science* **338**, 643-647 (2012).
3. H. S. Kim *et al.*, Lead iodide perovskite sensitized all-solid-state submicron thin film mesoscopic solar cell with efficiency exceeding 9%. *Sci. Rep.* **2**, 591 (2012).
4. J. Burschka *et al.*, Sequential deposition as a route to high-performance perovskite-sensitized solar cells. *Nature* **499**, 316-319 (2013).
5. N. J. Jeon *et al.*, Solvent engineering for high-performance inorganic-organic hybrid perovskite solar cells. *Nat. Mater.* **13**, 897-903 (2014).
6. N. Ahn *et al.*, Highly Reproducible Perovskite Solar Cells with Average Efficiency of 18.3% and Best Efficiency of 19.7% Fabricated via Lewis Base Adduct of Lead(II) Iodide. *J. Am. Chem. Soc.* **137**, 8696-8699 (2015).
7. E. H. Jung *et al.*, Efficient, stable and scalable perovskite solar cells using poly(3-hexylthiophene). *Nature* **567**, 511-515 (2019).
8. T. H. Han *et al.*, Surface-2D/Bulk-3D Heterophased Perovskite Nanograins for Long-Term-Stable Light-Emitting Diodes. *Adv. Mater.* **32**, e1905674 (2020).
9. B. Kim, S. I. Seok, Molecular aspects of organic cations affecting the humidity stability of perovskites. *Energy Environ. Sci.***13**, 805-820 (2020).
10. R. Wang *et al.*, A Review of Perovskites Solar Cell Stability. *Adv. Funct. Mater.* **29**, (2019).
11. N. Ahn *et al.*, Trapped charge-driven degradation of perovskite solar cells. *Nat. Commun.* **7**, 13422 (2016).
12. J. Yoon *et al.*, Superflexible, high-efficiency perovskite solar cells utilizing graphene electrodes: towards future foldable power sources. *Energy Environ. Sci.* **10**, 337-345 (2017).
13. G. Lee *et al.*, Ultra-flexible perovskite solar cells with crumpling durability: toward a wearable power source. *Energy Environ. Sci.***12**, 3182-3191 (2019).

14. T. Leijtens, K. A. Bush, R. Prasanna, M. D. McGehee, Opportunities and challenges for tandem solar cells using metal halide perovskite semiconductors. *Nat. Energy* **3**, 828-838 (2018).
15. L. Shen *et al.*, A Self-Powered, Sub-nanosecond-Response Solution-Processed Hybrid Perovskite Photodetector for Time-Resolved Photoluminescence-Lifetime Detection. *Adv. Mater.* **28**, 10794-10800 (2016).
16. L. Dou *et al.*, Solution-processed hybrid perovskite photodetectors with high detectivity. *Nat. Commun.* **5**, 5404 (2014).
17. J.-P. Correa-Baena *et al.*, Promises and challenges of perovskite solar cells. *Science* **358**, 739-744 (2017).
18. Y. Yuan, J. Huang, Ion Migration in Organometal Trihalide Perovskite and Its Impact on Photovoltaic Efficiency and Stability. *Acc. Chem. Res.* **49**, 286-293 (2016).
19. S. Ghosh, S. K. Pal, K. J. Karki, T. Pullerits, Ion Migration Heals Trapping Centers in CH3NH3PbBr3 Perovskite. *ACS Energy Lett.* **2**, 2133-2139 (2017).
20. A. J. Barker *et al.*, Defect-Assisted Photoinduced Halide Segregation in Mixed-Halide Perovskite Thin Films. *ACS Energy Letters* **2**, 1416-1424 (2017).
21. K. Domanski *et al.*, Migration of cations induces reversible performance losses over day/night cycling in perovskite solar cells. *Energy Environ. Sci.***10**, 604-613 (2017).
22. D. J. Slotcavage, H. I. Karunadasa, M. D. McGehee, Light-Induced Phase Segregation in Halide-Perovskite Absorbers. *ACS Energy Lett.* **1**, 1199-1205 (2016).
23. S. Tan *et al.*, Steric Impediment of Ion Migration Contributes to Improved Operational Stability of Perovskite Solar Cells. *Adv. Mater.* **32**, e1906995 (2020).
24. M.-c. Kim *et al.*, Degradation of CH3NH3PbI3 perovskite materials by localized charges and its polarity dependency. *J.Mater. Chem. A* **7**, 12075-12085 (2019).
25. K. Kwak *et al.*, An atomistic mechanism for the degradation of perovskite solar cells by trapped charge. *Nanoscale* **11**, 11369-11378 (2019).
26. N. Aristidou *et al.*, Fast oxygen diffusion and iodide defects mediate oxygen-induced degradation of perovskite solar cells. *Nat. Commun.* **8**, 15218 (2017).
27. J. Byeon *et al*, Charge transport layer dependent electronic band bending in perovskite solar cells and its correlation to device degradation, *ACS Energy Lett.* **5**, 2580-2589 (2020)
28. Y. Lin *et al.*, Excess charge-carrier induced instability of hybrid perovskites. *Nat. Commun.* **9**, 4981 (2018).
29. W. Nie *et al.*, Light-activated photocurrent degradation and self-healing in perovskite solar cells. *Nat. Commun.* **7**, 11574 (2016).
30. S. G. Motti *et al.*, Controlling competing photochemical reactions stabilizes perovskite solar cells. *Nat. Photonics* **13**, 532-539 (2019).
31. D. Bryant *et al.*, Light and oxygen induced degradation limits the operational stability of methylammonium lead triiodide perovskite solar cells. *Energy Environ. Sci.***9**, 1655-1660 (2016).

32. T. Duong *et al.*, Light and Electrically Induced Phase Segregation and Its Impact on the Stability of Quadruple Cation High Bandgap Perovskite Solar Cells. *ACS. Appl. Mater. Interfaces* **9**, 26859-26866 (2017).
33. P. Yadav, D. Prochowicz, E. A. Alharbi, S. M. Zakeeruddin, M. Grätzel, Intrinsic and interfacial kinetics of perovskite solar cells under photo and bias-induced degradation and recovery. *J. Mater. Chem. C* **5**, 7799-7805 (2017).
34. R. G. Balakrishna, S. M. Kobosko, P. V. Kamat, Mixed Halide Perovskite Solar Cells. Consequence of Iodide Treatment on Phase Segregation Recovery. *ACS Energy Lett.* **3**, 2267-2272 (2018).
35. M. V. Khenkin *et al.*, Dynamics of Photoinduced Degradation of Perovskite Photovoltaics: From Reversible to Irreversible Processes. *ACS Appl. Energy Mater.* **1**, 799-806 (2018).
36. S. G. Motti *et al.*, Photoinduced Emissive Trap States in Lead Halide Perovskite Semiconductors. *ACS Energy Lett.* **1**, 726-730 (2016).
37. D. A. Jacobs *et al.*, Hysteresis phenomena in perovskite solar cells: the many and varied effects of ionic accumulation. *Phys. Chem. Chem. Phys.* **19**, 3094-3103 (2017).
38. C. Eames *et al.*, Ionic transport in hybrid lead iodide perovskite solar cells. *Nat. Commun.* **6**, 7497 (2015).
39. D. Meggiolaro *et al.*, Iodine chemistry determines the defect tolerance of lead-halide perovskites. *Energy Environ. Sci.* **11**, 702-713 (2018).
40. X. Zhang, M. E. Turiansky, J.-X. Shen, C. G. Van de Walle, Iodine interstitials as a cause of nonradiative recombination in hybrid perovskites. *Phys. Rev. B* **101**, (2020).
41. L. D. Whalley, R. Crespo-Otero, A. Walsh, H-Center and V-Center Defects in Hybrid Halide Perovskites. *ACS Energy Lett.* **2**, 2713-2714 (2017).
42. E. Mosconi, D. Meggiolaro, H. J. Snaith, S. D. Stranks, F. De Angelis, Light-induced annihilation of Frenkel defects in organo-lead halide perovskites. *Energy Environ. Sci.***9**, 3180-3187 (2016).
43. S. van Reenen, M. Kemerink, H. J. Snaith, Modeling Anomalous Hysteresis in Perovskite Solar Cells. *J.Phys.Chem.Lett.* **6**, 3808-3814 (2015).
44. Zhang, T. et al. Understanding the relationship between ion migration and the anomalous hysteresis in high-efficiency perovskite solar cells: A fresh perspective from halide substitution. *Nano Energy* **26**, 620-630, (2016).
45. Buin, A. *et al.* Materials Processing Routes to Trap-Free Halide Perovskites. *Nano Lett.* **14**, 6281-6286, doi:10.1021/nl502612m (2014).
46. Khanna, V., Das, B. K., Bisht, D., Vandana & Singh, P. K. A three diode model for industrial solar cells and estimation of solar cell parameters using PSO algorithm. *Renew. Energy* **78**, 105-113 (2015).
47. Nishioka, K., Sakitani, N., Uraoka, Y. & Fuyuki, T. Analysis of multicrystalline silicon solar cells by modified 3-diode equivalent circuit model taking leakage current through periphery into consideration. *Sol. Energy Mater. Sol. Cells* **91**, 1222-1227, (2007).

Figures

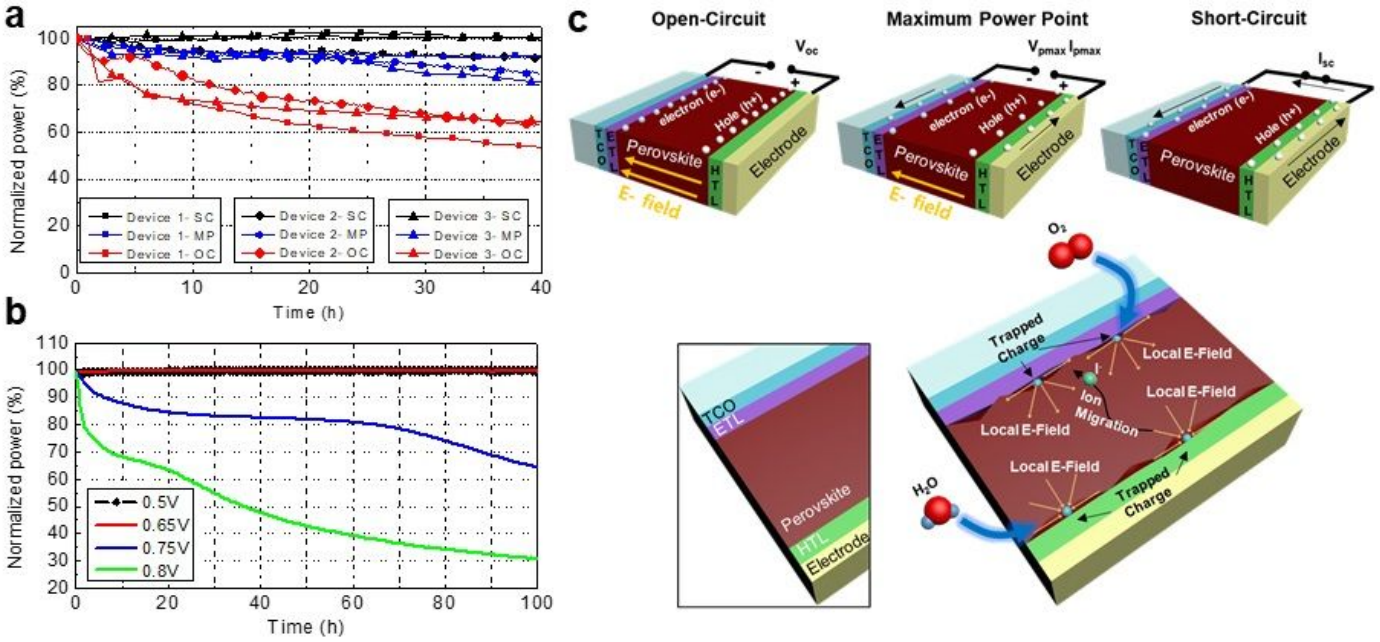

Figure 1

Bias-dependent degradation of perovskite solar cells a, Time evolution of the normalized power of three different devices measured at SC (short circuit), MPPT (maximum power point tracking) and OC (open circuit) condition under one sun illumination in ambient condition (30% of Relative humidity). All devices were glass-encapsulated. I-V scans were done every five hours. b, Time evolution of the normalized power of the device 3 measured at four different voltage biases around MPP (maximum power point). 0.5 V (black), 0.65 V (red), 0.75 V (blue), 0.8V (green). Normalized power was estimated from the multiplication of photocurrent and applied voltage bias. c, A schematic illustration describing the effect of voltage bias on charge accumulation, ion migration, and the resulting degradation. At the open-circuit condition, more charges accumulate at interfaces and strong e-field is formed across the perovskite film, leading to trapped-charge driven degradation and ion instabilities due to easy migration of ion defects. Even the trapped charges can induce ion migration and segregation as a result of localized electric field by themselves, which means that both charges and ions interplay as a strong source driving degradation.

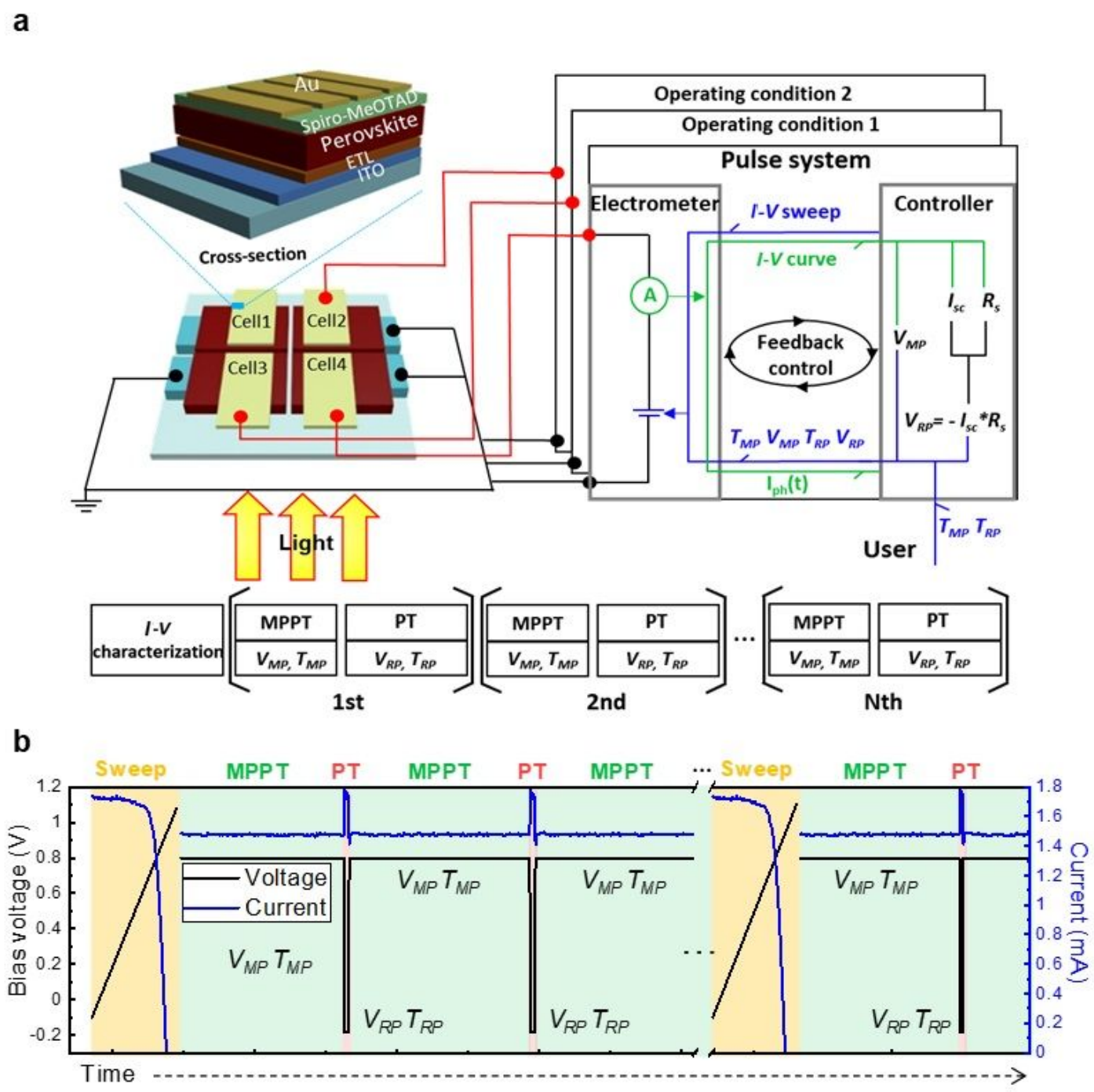

Figure 2

Pulsatile therapy for perovskite solar cells a, A schematic illustration of our novel system for pulsatile therapy and its basic algorithm. The system consists of a solar simulator, an electrosourcemeter, and a controller. The system was built to work automatically by the controller. Up to four cells under light illumination and different operating conditions can be tested at the same time. Pure MPPT operation is also available in this system. Each cell was electrically insulated. The operation steps of the pulsatile therapy consist of I-V scans, maximum power point tracking (MPPT), and short pulsatile therapy (PT). The MPPT and PT steps reiterate between I-V scans. Applied biases for MPPT and PT steps are updated after I-V scans from newly measured I-V curves and resulting photovoltaic parameters. The bias voltage

for the PT step is specially designed to extract charges and redistribute ions. Time intervals for all steps are initially set up prior to device test. The system stores real-time photocurrent and applied bias during the whole operation. b, The profile of applied bias voltage and corresponding photocurrent over time stored in our system. To heal a working device, the reverse pulses (VRP=-IscRs) were applied during the middle of MPPT. All parameters were calculated automatically in the controller. V MP : Maximum power point voltage, TMP : Time duration for maximum power point voltage, VRP: Reverse pulse voltage, TRP: Time duration for reverse pulse voltage. Isc : short-circuit current, Rs : series resistance

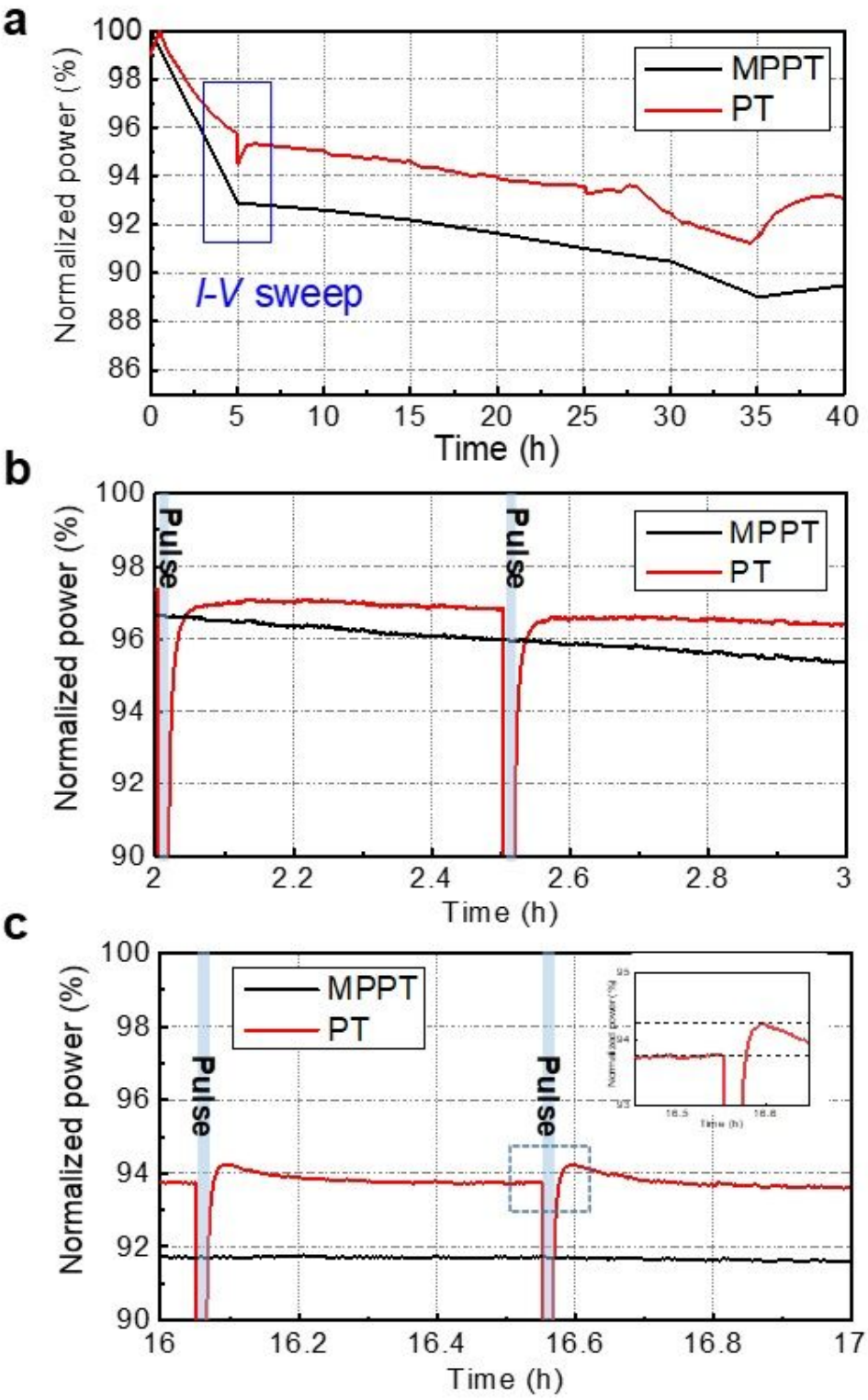

Figure 3

Efficacies of pulsatile therapy a, Time evolution of normalized power for MPPT(black) and PT(red)-tested cells. In this test, the I-V sweep was done every five hours to update I-V characteristics of the target device. The sudden change of normalized power at around 5 h occurred due to the significant change in maximum power point of the target device. b,c, Profiles of normalized power for PT- and MPPT- tested cells during 2-3 h of operation time (b) and 16-17 h of operation time (c). When the reverse pulses were applied, the harvesting power became negative, indicating power consumption during reverse pulses. Those induce transient changes of normalized power for PT-tested cells. The inset image is the magnified profile of the selected region showing the effect of short pulse. The reversible recovery of normalized power was clearly observed shortly after the pulse.

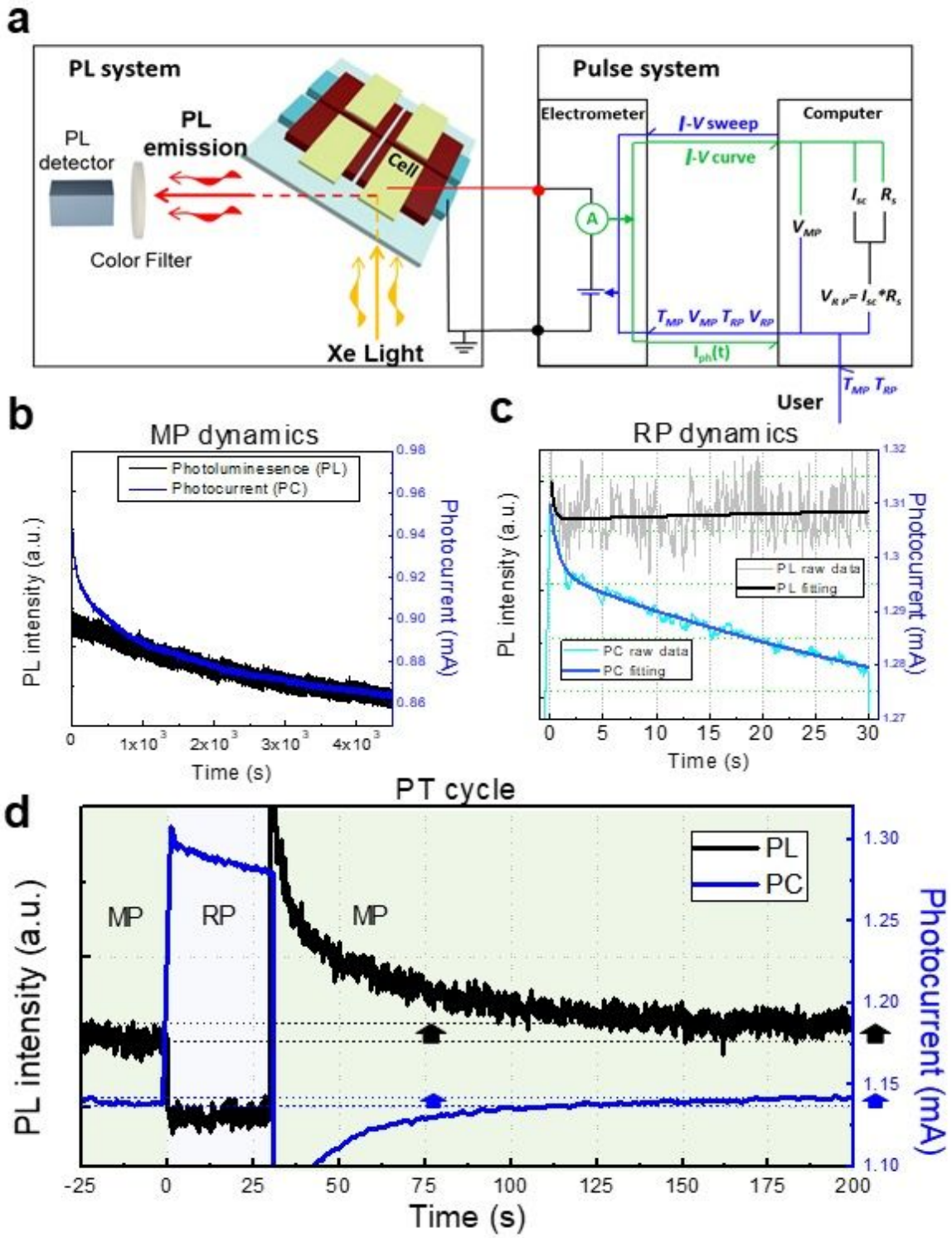

Figure 4

Defect healing mechanism underlying pulsatile therapy a, A schematic illustration of in-situ photoluminescence (PL) and photocurrent (PC) measurements combined with the PT system. The measurement setup was customized to investigate the effects of our pulsatile therapy. The sample was simultaneously controlled by the PT system, in which real-time photocurrent data was stored. The system enables to detect both PL and PC signals when the target device is under desired electrical operation,

which can provide dynamics of PL intensity and PC. b, Dynamics of PL intensity (black) and PC (blue) of the device operating under MPPT condition for over 4000 seconds. c, Dynamics of PL intensity (grey) and PC (cyan) of the PT-tested device during 30 seconds of pulsatile therapy after 30 minutes of MPPT operation. Both profiles for PL intensity (black) and PC (blue) were fitted by bi-exponential components with similar time-constants, indicating both dynamics would be governed by two factors, charge carriers and ions. The fast component indicates charge extraction and the slow component corresponds to ion movements d, Overall kinetics of PL intensity and PC during the pulsatile therapy (VMP-VRP-VMP). Both profiles were obtained by averaging PL intensity and PC data measured from three different cycles. Black and blue arrows point out restoration of PL intensity and PC, respectively, indicating device healing induced by short reverse pulses.

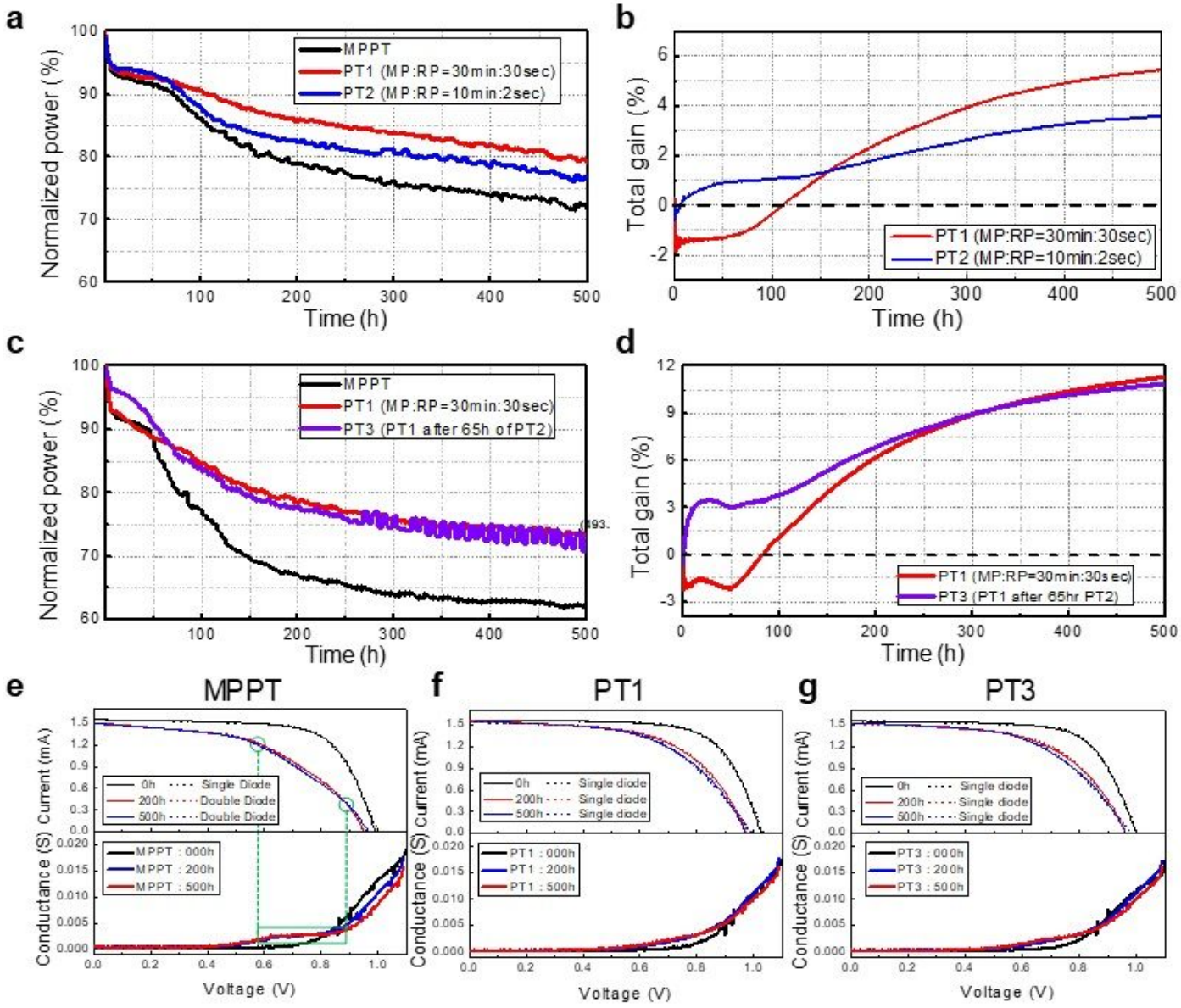

Figure 5

Long-term test a,b, Time evolution of normalized power (a) and total gain (b) of the devices working for 500 h under MPPT (black), PT1 (TMP:TRP = 30 min:30 sec) (red), and PT2 (TMP:TRP = 10min:2sec) (blue) under one sun illumination. Total gain means relative improvement of total energy generation of PT as compared to MPPT case. The dashed line is for 0% of total gain. c,d, Time evolution of normalized power (c) and total gain (d) of devices working for 500 h under MPPT (black), PT1 (TMP:TRP = 30min:30sec) (red), and PT3 (PT2 from 0h to 65h, PT1 from 65h to 500h) (violet). e,f,g, Histories of measured I-V curves (solid line) and simulated I-V curves (dashed line) of the devices working under MPPT (e), PT1 (TMP:TRP = 30min:30sec) (f), PT3 (PT2 from 0h to 65h, PT1 from 65h to 500h) (g) for t=0 h (black), 100 h (red) and 500 h (blue). In the case of MPPT, peculiar shape in the I-V curve and conductance-voltage curve of the device working for over 200 h appeared, showing two deflections in the curve. The peculiar I-V curves were simulated based on double-diode circuit modeling. The secondary diode corresponds to a new trap-assisted recombination pathway in the modeling.

Supplementary Files

This is a list of supplementary files associated with this preprint. Click to download.

- PulsatiletherapyforperovskitesolarcellsSupplementaryInformation.docx
- ExtendedDataFile.pdf